# Scalable and Environmentally Friendly MXene-Tetrahedrites for Next-Generation Flexible Thermoelectrics

Priyanshu Banerjee,[a*] Jiyuan Huang,[a*] Jacob Lombardo,[a] Swapnil B. Ambade,[b] Rohan B. Ambade,[c,d,e,f] Tae Hee Han,[c,d] Srushti Kulkarni,[a] Shreyasi Sengupta,[g] Zeev Rosenzweig,[g] Howard Fairbrother,[b] Sichao Li,[h] Sunmi Shin,[h] Deepa Madan[a,**]

[a]Department of Mechanical Engineering, University of Maryland Baltimore County, Baltimore, MD 21250, USA

[b]Department of Chemistry, Johns Hopkins University, Baltimore, MD 21205, USA

[c]Department of Organic and Nano Engineering, Hanyang University, Seoul 04763, Republic of Korea

[d]The Research Institute of Industrial Science, Hanyang University, Seoul 04763, Republic of Korea

[e]Advanced Research & Innovation Center, Khalifa University of Science & Technology, 127788, Abu Dhabi, United Arab Emirates

[f]Department of Aerospace Engineering, Khalifa University of Science & Technology, 127788, Abu Dhabi, United Arab Emirates

[g]Department of Chemistry and Biochemistry, University of Maryland Baltimore County, Baltimore, MD 21250, USA

[h]Department of Mechanical Engineering, Collage of Design and Engineering, National University of Singapore

* These authors contributed equally to this work
**Corresponding Author, E-mail: deemadan@umbc.edu

# Contents

**Table S1.** Room-temperature comparison of electrical conductivity, Seebeck coefficient, power factor, thermal conductivity, and ZT for Chitosan-TE composite films versus other binder-based composites in existing literature.

**Table S2.** Room-temperature comparison of electrical conductivity, Seebeck coefficient, power factor, thermal conductivity, and ZT for bulk $Cu_{12}Sb_4S_{13}$ pellets from literature versus Chitosan-CAS and Chitosan-CAS-MXene TE composite films measured at room-temperature.

**Table S3.** Binding energy and oxidation states for the XPS peaks for the elements present in Chitosan-CAS-MXene TE film, Chitosan-CAS TE Film, CAS powder.

**Table S4.** Comparison of printed TEG device performance between previous reports and this work.

## TE properties measurement and characterization

The in-plane electrical conductivity, carrier concentration, and mobility measurements were carried out in ambient conditions using the Hall Effect Measurement System (ECOPIA, HMS-5500).[1-7] A custom-built Seebeck measurement setup was used to measure the Seebeck coefficient of the TE composite films.[4-13] The thermal conductivity was measured in both in-plane and out-of-plane directions.[1-3,11,13] The in-plane measurement was carried out using the well-established 3ω method to provide reliable thermal conductivity of films.[14-16] The AC-modulated heating can control the penetration depth by controlling the frequency. Additionally, operating within an ultra-high vacuum environment minimizes convective heat transfer by the air.[15] Furthermore, the temperature rise was controlled to be less than 11K to minimize potential error by the temperature-dependent thermal conductivity.

## Thermal conductivity measurement based on the AC modulated 3ω method

To evaluate the free-standing Chitosan-CAS and Chitosan-CAS-MXene samples cross-plane thermal conductivity, we measured the thermal conductivity based on the well-acknowledged AC modulated 3ω method. Au electrodes (as a heater and a sensor simultaneously) were deposited onto a thin layer of PDMS, which was then transferred onto the free-standing Chitosan-CAS and Chitosan-CAS-MXene samples. The PDMS layer, acting as an electric insulating layer and a substrate to enable the transferring process, had a relatively thin thickness of approximately 40 μm compared to the sample thickness of around 300 μm. Subsequently, the heaters were manually bonded on the chip carrier and connected to the external circuit. To ensure measurement accuracy, we conduct the measurement in a vacuum chamber ($<10^{-5}$ Torr) to minimize heat convection. AC-modulated joule heating induced the temperature rise at the Au

heater, while the resistance change was detected by the 3rd harmonic voltage signal, corresponding to the temperature rise. The heating frequency was varied from 2 Hz to 2000 Hz to control the thermal penetration depth ($L_P$), defined by $L_P = \sqrt{\frac{\kappa}{\rho C_p \omega}}$, where $\kappa$ is the thermal conductivity, $\rho$ is density, $C_p$ indicates the specific heat, and $\omega$ represents the angular frequency of the heat current. At a higher frequency range, when the thermal penetration depth is limited within the PDMS layer, we only detect the PDMS thermal conductivity of around 0.24 W/m-K. Further increasing the $L_P$ by reducing the frequency of the heating current (2 Hz to 7 Hz), the $L_P$ can be extended into the sample layer, allowing us to determine the thermal conductivity of Chitosan-CAS and Chitosan-CAS-MXene samples using a previously developed analytical model. [15,16]

The density measurement was performed separately by weight and voltage measurements. The weight was measured by a balance (SARTORIUS, TE214S Analytical Balance), and the voltage was measured by a 3D laser scanning microscope (KEYENCE, VX-X1000). [1,3,5,6]

**Physical Characterization**

X-ray diffraction (XRD) analysis was completed to show the corresponding peaks of pure MXene, CAS powder, Chitosan-CAS TE composite films, and Chitosan-CAS-MXene TE composite films. The XRD analysis employed a Cu-Kα radiation source on a Rigaku mini flex operating at 15 mA and 30 kV. X-ray photoelectron spectroscopy (XPS) analysis was performed to study the formation of bonds between CAS, MXene, and Chitosan in Chitosan-CAS and Chitosan-CAS-MXene TE composite films as well as the chemical states of CAS powder and pristine MXene. Raman analysis was conducted to show the peaks corresponding to Chitosan-CAS and Chitosan-CAS-MXene composite films, CAS powder, and pure MXene. Changes in the full width at half maximum (FWHM) and Raman shift of phonon modes (phonon softening)

illustrate changes in DOS effective mass, weighted mobility, and phonon vibrations caused by introducing dislocations and interfaces with pressure.[17-19] The study of the surface microstructure of the TE composite films as well as particle-size distribution of CAS powder, pure MXene, and Chitosan-CAS TE composite films as well as Chitosan-CAS-MXene TE composite films was carried out using field emission scanning electron microscopy (SEM/FESEM) and high-resolution transmission electron microscopy (HRTEM). The SEM/FESEM images of Chitosan-CAS-MXene TE composite films were taken using Zeiss/Nova NanoSEM 450 (FEI). Additionally, the presence of nano-defects and interfaces between MXene, CAS particles, and Chitosan binder in both Chitosan-CAS and Chitosan-CAS-MXene TE composite films were characterized using HRTEM. The elemental composition study on all four samples used energy-dispersive X-ray spectroscopy (EDAX/EDS). TEM, HRTEM, and EDAX were performed using JEM2100F at an operating voltage of 200 kV using a working voltage of 8 V and a working distance of 3 mm. Selected area diffraction (SAED) was employed to study the orientation, lattice spacing, and crystalline information of CAS and MXene in both Chitosan-CAS and Chitosan-CAS-MXene TE composite films. Brunauer–Emmett–Teller (BET) and Barrett–Joyner–Halenda (BJH) properties were analyzed using nitrogen ($N_2$) adsorption (BELSORP-MAX) to estimate the surface area, volume, and pore size of both Chitosan-CAS and Chitosan-CAS-MXene TE composite films. The $N_2$ adsorption-desorption isotherms were carried out at 77 K. UV-visible spectrophotometry (UV-VIS) was completed to illustrate the band gap, and Ultraviolet photoelectron spectroscopy (UPS) was completed to analyze the work function interface potential, as well as the distance between the Fermi level and the valence bands in CAS powder, 2D MXene Nanosheets, as well as Chitosan-CAS and Chitosan-CAS-MXene composite films. The energy band diagram (**Figure 6**) shows the

formation of an energy barrier at the Chitosan-CAS/MXene interface through UPS and UV-Vis analysis (**Figure 6, S5**), decoupling electrical conductivity with the Seebeck coefficient. [20,21]

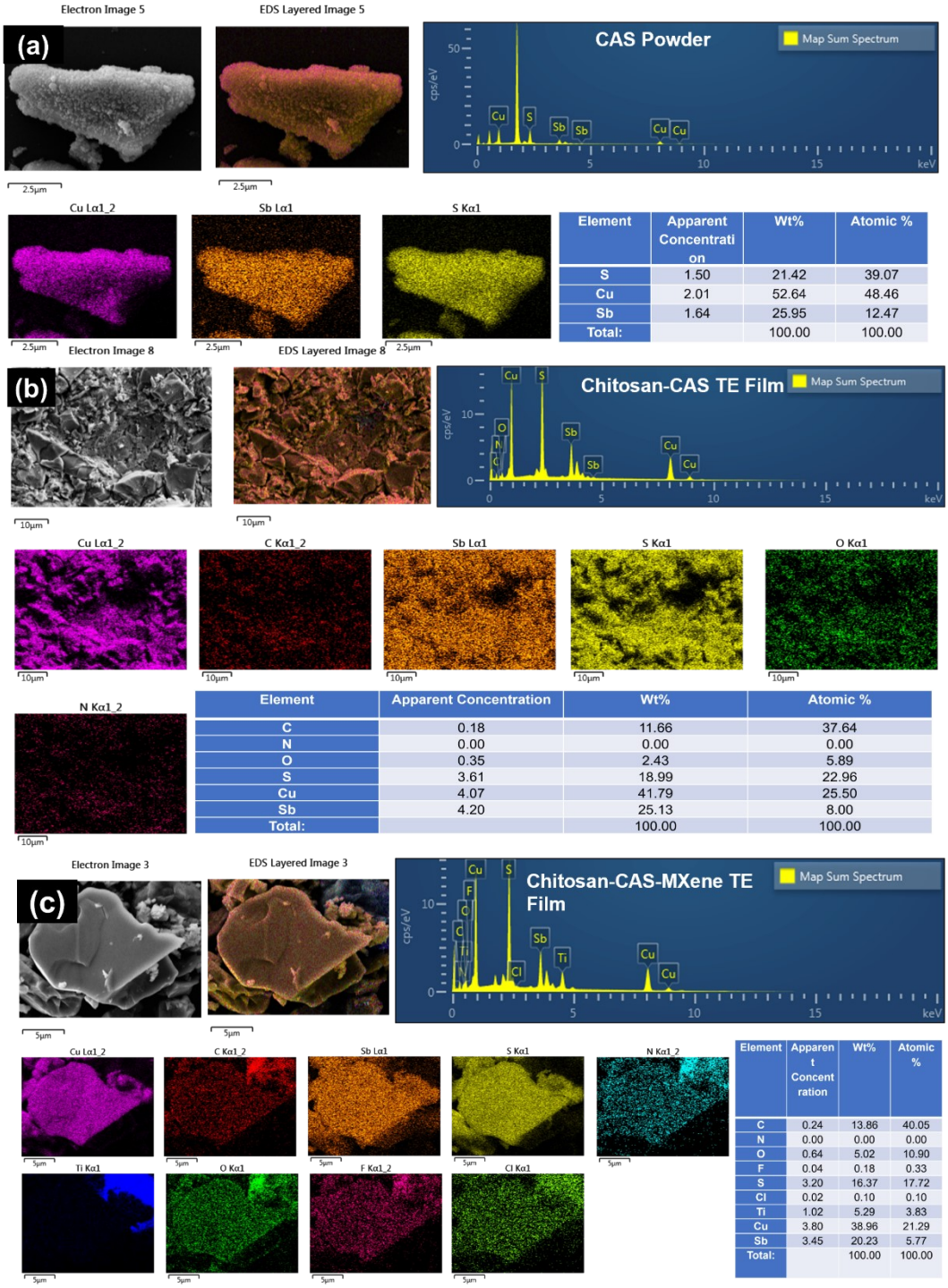


**Figure S1.** EDAX, TEM image with its corresponding elemental mapping and a data table illustrating elemental concentrations in terms of wt.% and at.% for (a) CAS powder, (b) Chitosan-CAS, and (c) Chitosan-CAS-MXene TE film.

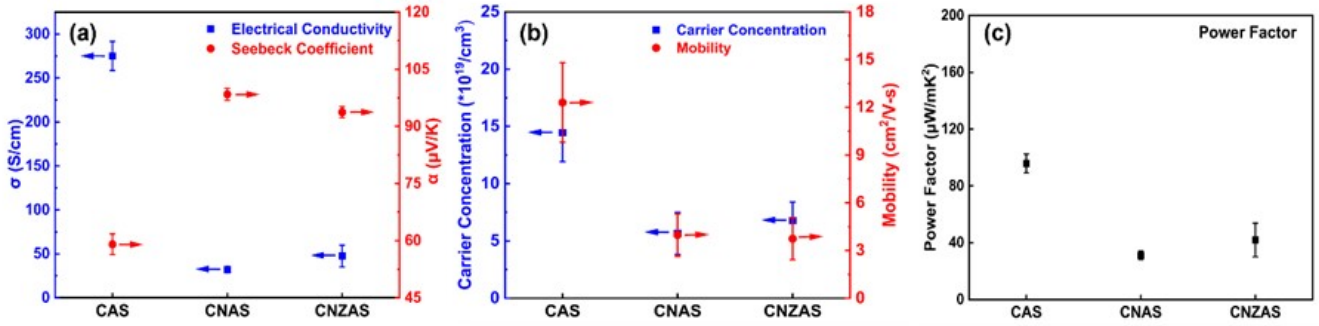


**Figure S2.** Room temperature (a) Electrical conductivity and Seebeck coefficient (b) Carrier concentration and mobility (c) Power Factor of Chitosan-CAS (325-mesh, 0.01 wt.%) TE composite films using three different tetrahedrite compositions (CAS, CNAS, and CNZAS)

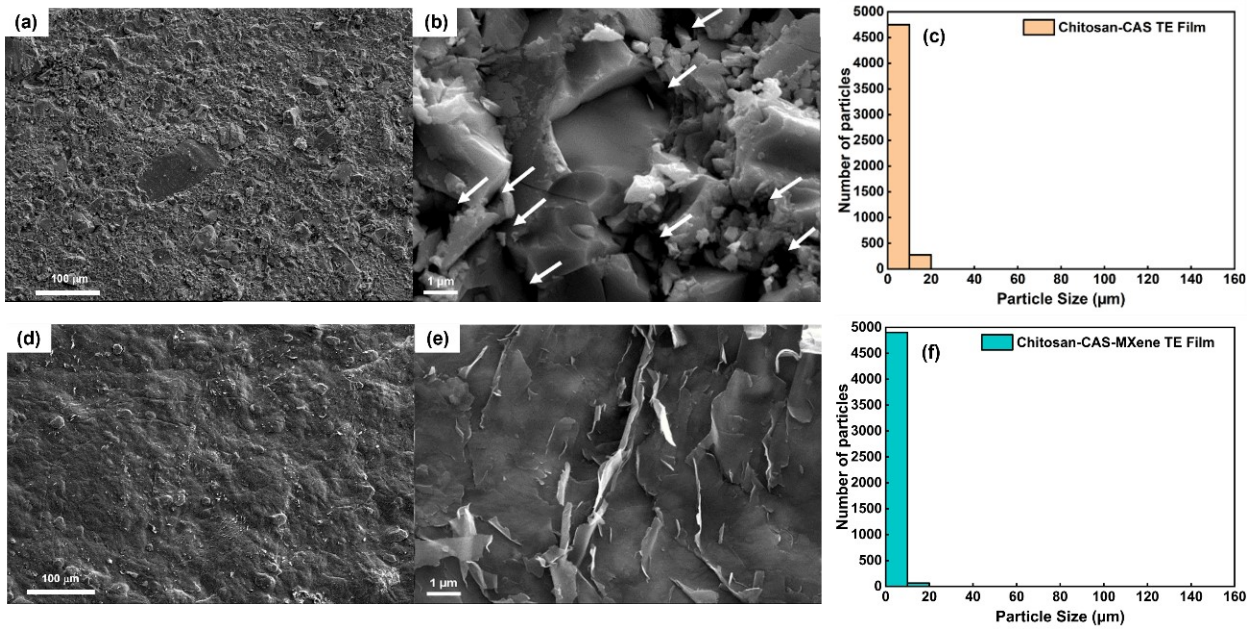


**Figure S3.** (a,b) FESEM images of Chitosan-CAS composite films, (c) ImageJ analysis of Micron-sized TE particle count *vs*. particle size of Chitosan-CAS film, (d,e) FESEM images of Chitosan-CAS-MXene composite films, and (f) ImageJ analysis of Micron-sized TE particle count *vs*. particle size of Chitosan-CAS film.

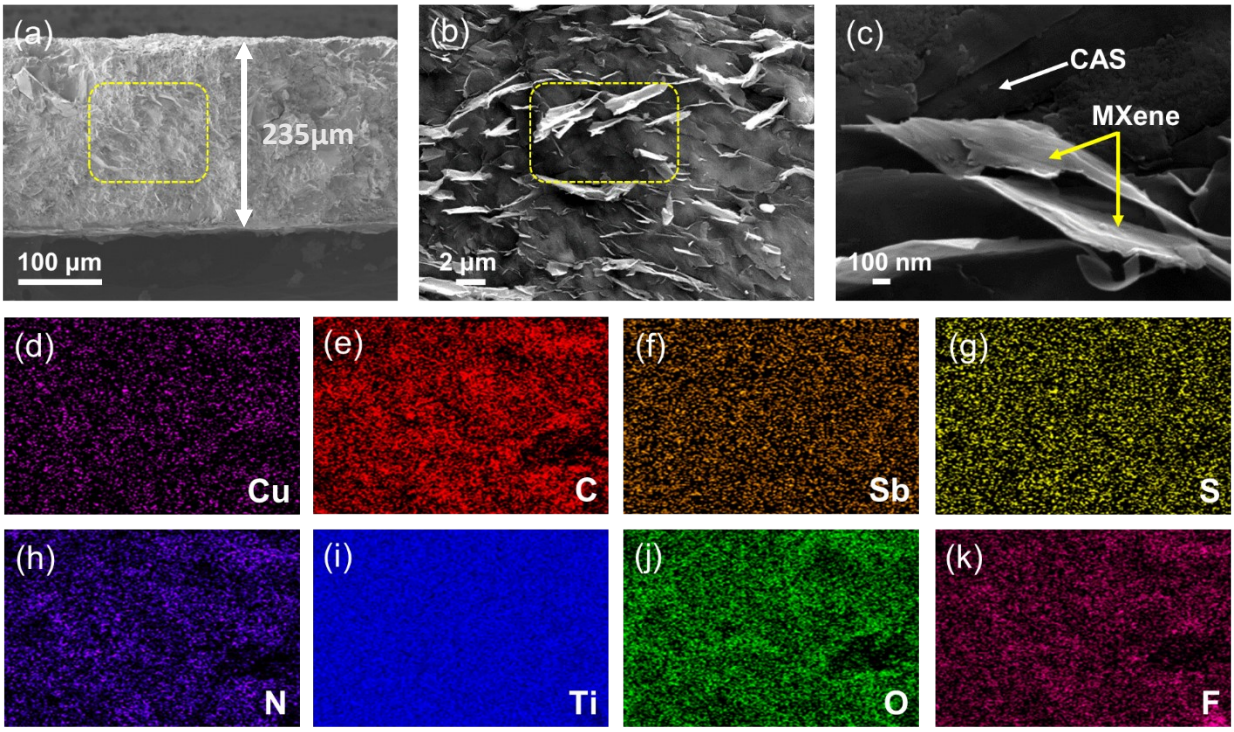


**Figure S4**. (a-c) Cross-section images of Chitosan-CAS-MXene TE film, and (d-k) EDAX elemental mapping of Chitosan-CAS-MXene TE film.

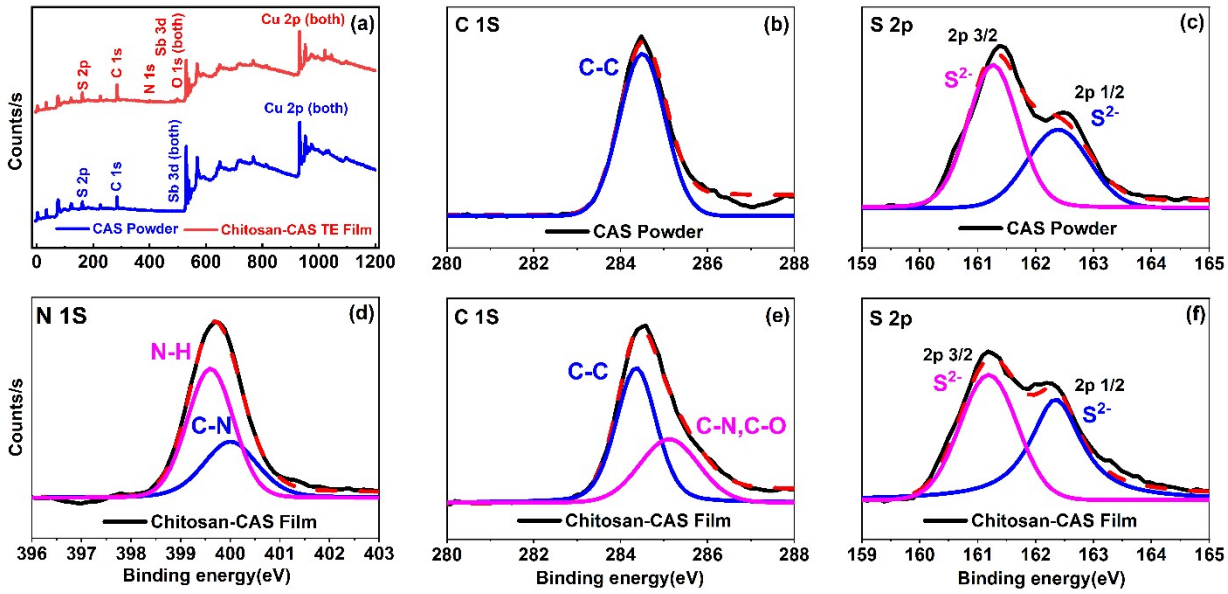


**Figure S5.** (a) Full XPS Spectra for Chitosan-CAS TE Film and CAS Powder, (b) C 1s for CAS Powder, (c) S 2p for CAS Powder, (d) N 1s for Chitosan CAS Film, (e) C 1s for Chitosan-CAS Film, (f) S 2p for Chitosan-CAS TE Film and CAS Powder.

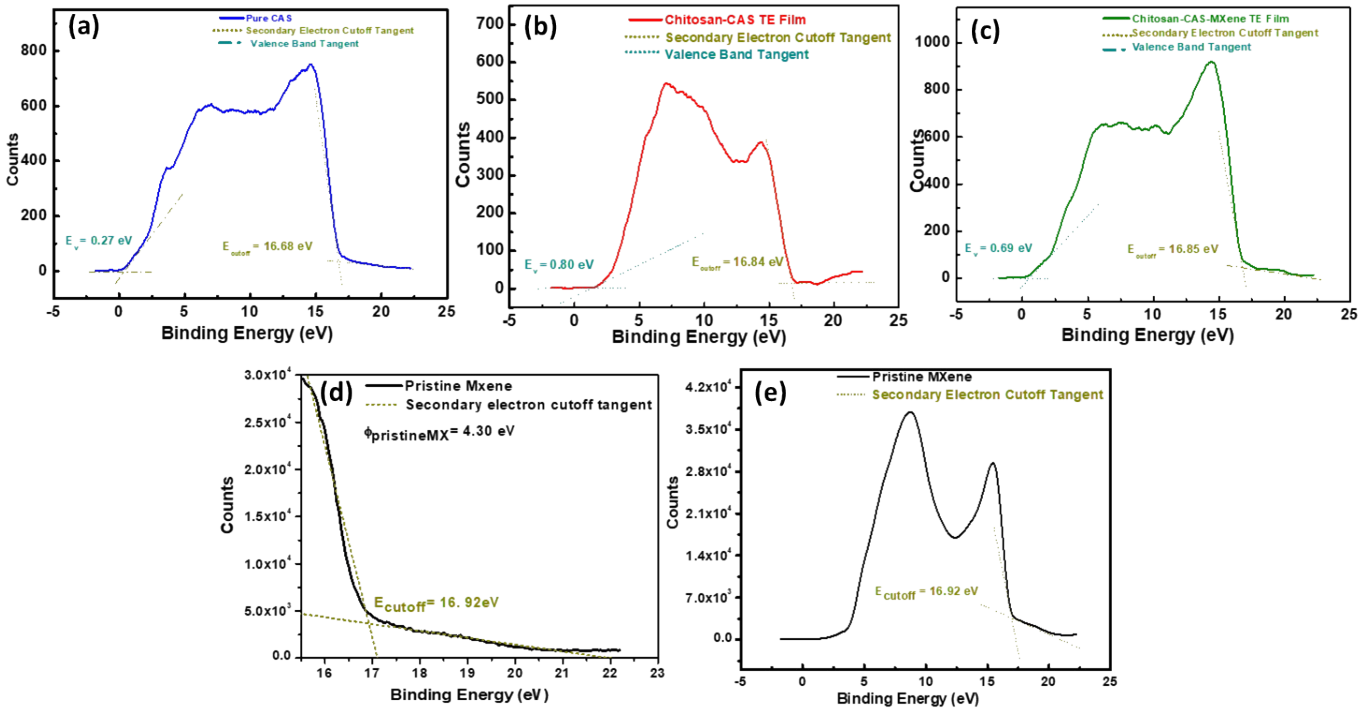


**Figure S6.** Wide range UPS (He I: 21.21 eV) spectrum of (a) CAS Powder, (b) Chitosan-CAS, (c) Chitosan-CAS-MXene TE film. UPS spectra of (d) Pure MXene at the secondary edge region for direct determination of the work function and (e) its corresponding wide range spectrum (He I: 21.21 eV).

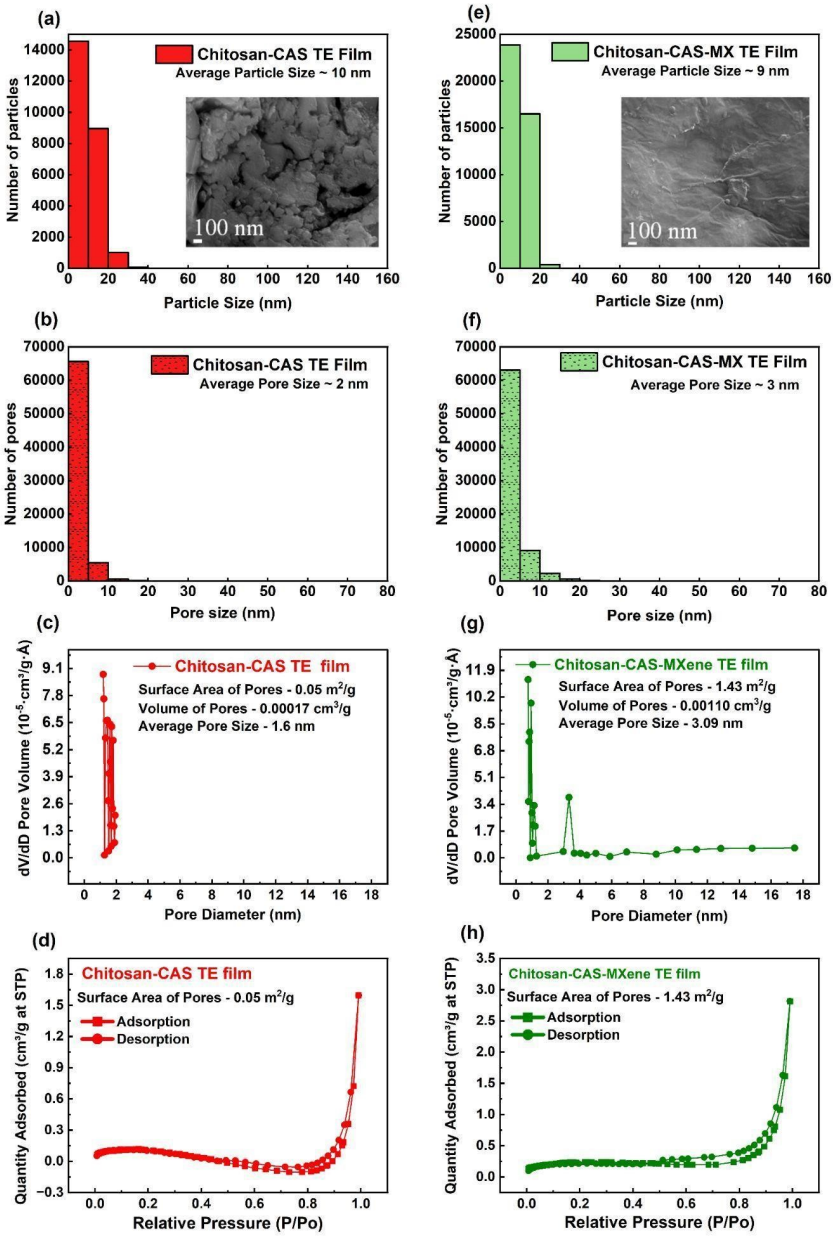


**Figure S7.** Nano-sized TE particle count *vs.* particle size using ImageJ software of (a) Chitosan-CAS TE composite films, (e) Chitosan-CAS-MXene TE composite film with their corresponding FESEM images in the inset. Nanoscale pore count *vs.* pore size, using ImageJ software for counting the pores of (b) Chitosan-CAS TE composite films and (f) Chitosan-CAS-MXene TE composite films. Pore size distribution of (c) Chitosan-CAS TE composite films and (g) Chitosan-CAS-MXene TE composite films were obtained from a BET analysis. Nitrogen adsorption-desorption isotherms of (d) Chitosan-CAS TE composite films and (h) Chitosan-CAS-MXene TE composite films.

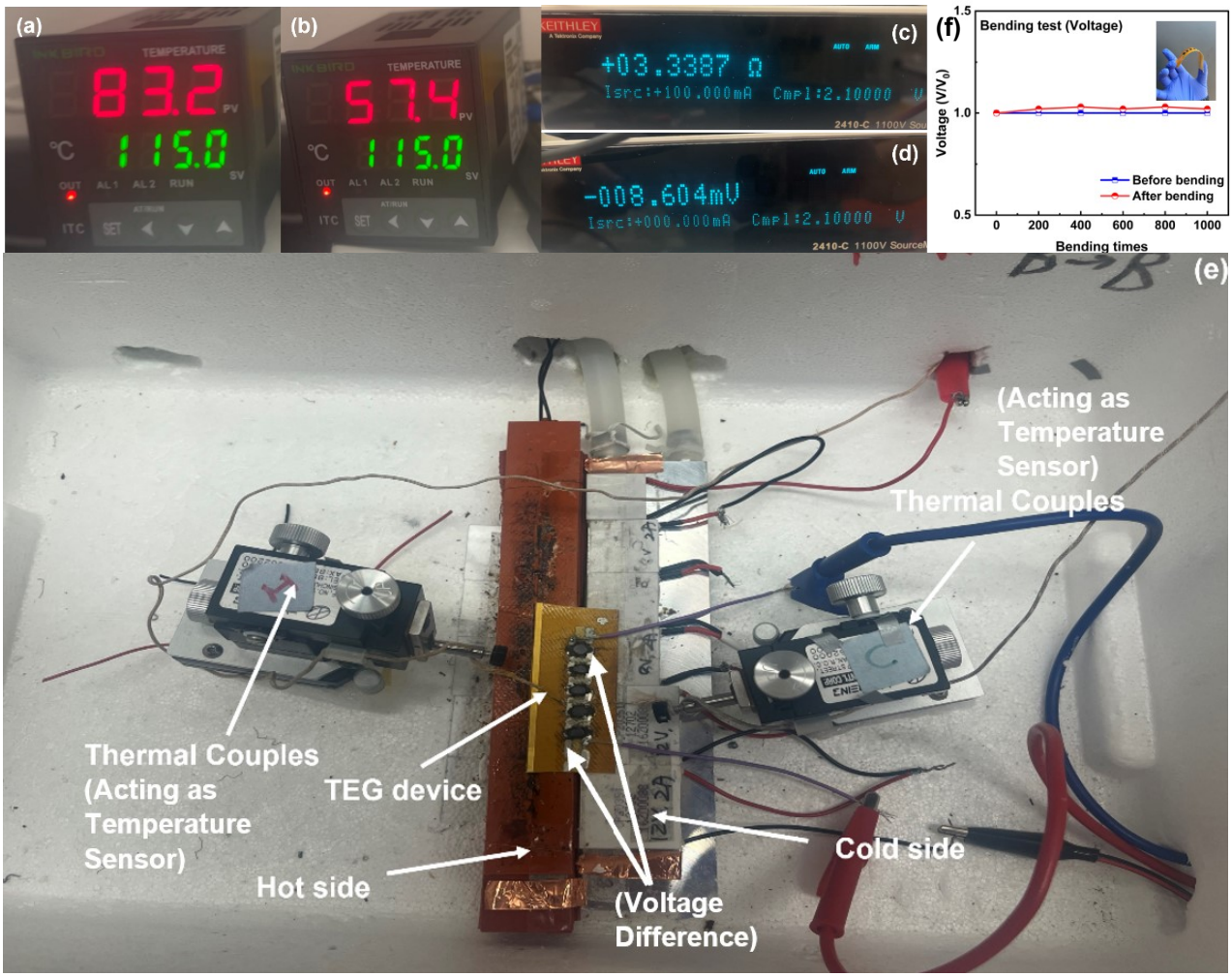


**Figure S8.** (a, b) TEG device setup showing temperature difference, (c) internal device resistance, (d) open-circuit voltage output, and (e) device setup, (f) Normalized open circuit voltage of TEG *vs.* bending cycles, $V_0$ and V, is open circuit voltage before and after bending.

**Table S1.** Room-temperature comparison of electrical conductivity, Seebeck coefficient, power factor, thermal conductivity, and ZT for Chitosan-TE composite films versus other binder-based composites in existing literature.

| Material | Binder | Electrical conductivity (S/cm) | Seebeck Coefficient (μV/K) | Power Factor (μW/mK²) | Thermal Conductivity (W/m-K) | Figure of Merit (ZT) | Ref. |
|---|---|---|---|---|---|---|---|
| p-BST | Chitosan | 600 | 174 | 2100 | 0.78 | 0.7 | 1 |
| p-BST<br>n-BTS | Chitosan | 660<br>286 | 186<br>194 | 2520<br>989 | 0.77<br>0.65 | 0.89<br>0.5 | 3 |
| p-Sb2Te3<br>n-Bi2Te3 | Removable binder | 1250<br>550 | 100<br>140 | - | 1.3<br>1.0 | 0.28<br>0.33 | 4 |
| p-BST<br>n-Bi2Te3 | chalcogenidometallate (ChaM) ions | 550<br>500 | 200<br>155 | - | 0.62<br>0.58 | 0.9<br>0.6 | 5 |
| p-BST<br>n-BTS | chalcogenidometallate (ChaM) ions | 700<br>650 | 170<br>120 | - | 0.5<br>0.53 | 1.21<br>0.67 | 6 |
| n-BTS | Removable binder | 477 | 190 | 1722 | 0.65 | 0.9 | 7 |
| p-Sb2Te3<br>n-Bi2Te3 | Epoxy resin 862 | 315<br>17 | 152<br>275 | 737<br>128 | 0.54<br>0.24 | 0.41<br>0.16 | 8 |
| n-Bi2Te3<br>+1%Se | Epoxy resin 862 | 140 | 200 | 470 | 0.38 | 0.31 | 9 |
| Sb2Te3 | NFC Hydrogel | 233 | 104 | 214 | - | n/a | 10 |
| n-BTS | Chitosan | 200 | 202 | 808 | 0.4 | 0.4 | 11 |
| Sb2Te3 | Epoxy resin 862 | 30 | 217 | 138 | - | n/a | 12 |
| Sb2Te3 | Epichlorohydrin polyglycol-based epoxy | 100 | 138.4 | 192 | 0.426 | 0.135 | 22 |
| Ca3Co4O9 | - | 142.8 | 133 | 232 | - | n/a | 23 |
| p-BST+8%Te | Epoxy polymer | 12 | 200 | 180 | 0.24 | 0.2 | 24 |
| n-BTS | Disperbyk-110 | 275 | 142 | 560 | 0.55 | 0.43 | 25 |
| p-BST | Disperbyk-110 | 700 | 204 | 3000 | 0.95 | 1 | 26 |
| p-BST<br>n-BTS | Removable binder | 700<br>570 | 195<br>190 | - | 0.92<br>0.95 | 0.93<br>0.64 | 27 |
| **$Cu_{12}Sb_4S_{13}$ + MXene** | Chitosan | **454** | **82** | **302** | **0.40** | **0.22** | **This work** |

**Table S2.** Room-temperature comparison of electrical conductivity, Seebeck coefficient, power factor, thermal conductivity, and ZT for bulk $Cu_{12}Sb_4S_{13}$ pellets from literature versus Chitosan-CAS and Chitosan-CAS-MXene TE composite films.

| Material | Electrical conductivity (S/cm) | Seebeck Coefficient (μV/K) | Power Factor (μW/mK²) | Thermal Conductivity (W/m-K) | Figure of Merit (ZT) | Fabrication method | Ref. |
|---|---|---|---|---|---|---|---|
| $Cu_{12}Sb_4S_{13}$ (Bulk TE pellets) | 400 | 85 | 289 | 1.3 | 0.08 | Individual elements of Cu, Sb, and S were mixed in an atomic ratio in vacuum ► heated at 923 K and held for 12 hours (1st annealing) ► slowly cooled to RT ► 1st Ball-milling (5 min) ► cold-pressing ► 2nd annealing (2 weeks @ 723 K) ► 2nd Ball-milling (30 min) ► sintering for 30 min. (703 K @ 80 MPa) | 28 |
| $Cu_{12}Sb_4S_{13}$ (Bulk TE pellets) | 1000 | 80 | 640 | 1.27 | 0.15 | Individual elements of Cu, Sb, and S were mixed in an atomic ratio in vacuum ► heated at 973 K (1st annealing) ► 2-step cooling (30 hr. @ 823 K followed by RT) ► 1st Ball-milling ► cold-pressing ► 2nd annealing (25 hr. @ 773 K) ► 2nd Ball-milling ► sintering for 1 hr. (803 K @ 60 MPa) | 29 |
| $Cu_{12}Sb_4S_{13}$ (Bulk TE pellets) | 500 | 115 | 661 | 0.95 | 0.2 | Individual elements of Cu, Sb, and S were mixed in an atomic ratio in vacuum ► heated to 973 K and held for 3 hr. (1st annealing) ► 2-step cooling (30 hr. @ 793 K followed by RT) ► 1st Ball-milling ► cold-pressing ► 2nd annealing (25 hr. @ 793 K) ► 2nd Ball-milling (crushed to 200 um) ► sintering for 30 min. (793 K @ 60 MPa) | 30 |
| **Chitosan-$Cu_{12}Sb_4S_{13}$ (TE composite film)** | **275** | **59** | **96** | **0.70** | **0.04** | Low thermal budget additive manufacturing method using $Cu_{12}Sb_4S_{13}$ 325 Mesh combined with Chitosan ink ► Sonicated for 30 min ► Cured (30 min @ 120C) ► Pressed (30 min @ 20 MPa) | **This work** |
| **Chitosan-$Cu_{12}Sb_4S_{13}$ - MXene (TE composite** | **454** | **82** | **302** | **0.41** | **0.22** | Low thermal budget additive manufacturing method using $Cu_{12}Sb_4S_{13}$ 325 Mesh combined with Chitosan ink ► Sonicated for 30 min ► Cured (30 | **This work** |

| | | | | | | | |
|---|---|---|---|---|---|---|---|
| **film)** | | | | | | min @ 120C) ► Pressed (30 min @ 20 MPa) ► (MXene drop cast ► Pressed (20 min @ 20 MPa))(3x) | |

**Table S3:** Binding energy and oxidation states for the XPS peaks for the elements present in Chitosan-CAS-MXene TE film, Chitosan-CAS TE Film, CAS powder.

| Elements | Peak | Binding Energy (in eV) | Oxidation State | BE (this work) |
|---|---|---|---|---|
| Cu | $2p_{1/2}$ | 951.7 | +1 | 951.86 |
| Cu | $2p_{3/2}$ | 932.3 | +1 | 932.25 |
| Cu | $2p_{1/2}$ | 953.3 | +2 | 953.7 |
| Cu | $2p_{3/2}$ | 933.1 | +2 | 933.8 |
| Sb | $3d_{3/2}$ | 538.0 | +3 | 539.4 |
| Sb | $3d_{5/2}$ | 528.21 | +3 | 530.1 |
| Sb | $3d_{5/2}$ | 527.0 | 0 | 528.4 |
| Sb | $3d_{3/2}$ | 536.2 | 0 | 537.8 |
| S | $2p_{1/2}$ | 161 | -2 | 161.2 |
| S | $2p_{3/2}$ | 162.8 | -2 | 162.4 |
| Ti-S | $2p_{3/2}$ | 160.90 | | 161.12 |
| Ti-S | $2p_{1/2}$ | 162.0 | | 162.40 |
| Ti-S | $2p_{3/2}$ | 456.2 | | 455.5 |
| Ti-S | $2p_{1/2}$ | 462.2 | | 463.8 |
| Ti-C | $2p_{3/2}$ | 454.9 | | 455.0 |
| Ti-O | $2p_{3/2}$ | 458.6 | | 458.5 |
| Ti-O | $2p_{1/2}$ | 464.7 | | 464.9 |
| N-H | 1s | 399.3 | | 399 |
| C-N-C | 1s | 403.9 | | 400 |
| C-N | 1s | 286.6 | | 285.2 |
| C-C | 1s | 284.5 | | 284.3 |

* Data reference NIST XPS database

**Table S4.** Comparison of printed TEG device performance between previous reports and this work.

| No. of elements | Internal resistance (W) | Max Power (μW) | ΔT (K) | Power density (mW/cm$^2$) | Reference |
|---|---|---|---|---|---|
| 3 | - | 58 | 38 | 3.5 | 1 |
| 9 | 12 | 73 | 40 | 0.566 | 2 |
| 12 | 6.9 | 357.6 | 40 | 5.0 | 3 |
| 8 | 0.35 | | 50 | 3.8 | 4 |
| 6 | 0.105 | 1620 | 39 | 1.42 | 5 |
| 4 | 8.5 | 54 | 80 | 18.8 | 26 |
| 152 | 685 | 406 | 47 | 1.84 | 27 |
| 10*10 | 22 | 173 | 19.7 | 0.15 | 31 |
| 7 | 200 | 2.26 | 30 | - | 32 |
| 24 | ~1600 | 0.015 | 35 | - | 33 |
| 254 | 25 | 3.14 | 123 | 0.029 | 34 |
| 20 | 140 | 8.42 | 20.9 | - | 35 |
| 4 | - | 0.141 | 50 | 2.7 | 36 |
| 40 | 130k | 0.08 | 75 | - | 37 |
| 40 | 200 | 6.5 | 25 | 0.000149 | 38 |
| 142 | 1.94 | 166 | 46.2 | 2.43 | 39 |
| 50 | - | 5.55 | 18.7 | 0.0061 | 40 |
| 48 | 300 | 2.61 | 22 | 0.003 | 41 |
| 16 | 7.2k | 0.04 | 20 | - | 42 |
| 14 | 8.5k | 0.21 | 30 | - | 43 |
| 4 | - | - | 70 | 0.22 | 44 |
| 200 | 380k | 0.032 | 40 | - | 45 |
| 50 | 2.33k | 10.5 | 20 | 0.075 | 46 |
| 10 | 100 | 130 | 70 | 1.23 | 47 |
| 5*10 | 55 | 33 | 20 | 0.28 | 48 |
| 8 | 592 | 0.444 | 20 | - | 49 |
| 50 | 55 | 33 | 20 | 0.28 | 50 |
| **5** | **3.3** | **5.3** | **25** | **0.14** | **This work** |

**Environmental Impact of CAS-Chitosan and Chitosan-CAS-MXene**

The impact of the CAS-Chitosan and CAS-MXene-Chitosan composite materials on the viability of *Shewanella oneidensis* MR-1, an environmentally relevant Gram-negative bacterium.[51-53], was measured to determine the potential environmental impact of these thermoelectric composite materials once released to the environment post use. Bacterial viability tests were conducted following a previously reported protocol of growth-based viability (GBV) assay.[52, 53] *Shewanella oneidensis* MR-1 106686 was stored at -80°C until use. The bacterial stock was plated on a sterilized Luria-Bertani (LB) agar plate and incubated at 30°C overnight. The resulting bacterial colonies were inoculated in 10 mL of LB media and incubated in an orbital shaker at 30°C and 250 rpm for 4-6 hours or until the mid-log phase (optical density at 600 nm or $OD_{600}$~0.5). Next, the culture was centrifuged at 1000 x *g* for 10 minutes, resuspended with 0.2 M phosphate-buffered saline (PBS), and centrifuged again at 1000 x *g* for 10 minutes. The pellet was resuspended in HEPES buffer (2 mM HEPES, 25 mM NaCl, pH=7.4) to obtain a $OD_{600}$ value of ~0.1. In a 96-well plate, the bacteria were exposed to the thermoelectric composite materials namely CAS-Chitosan and CAS-MXene-Chitosan at concentrations ranging from 0 to 600 mg/L, as well as an antibiotic, kanamycin at concentrations (0, 20, 50) mg/L for 1 h. After the exposure, a 5 L of each suspension was removed and added to 195 L of fresh LB broth in a new 96-well plate in triplicates. $OD_{600}$ was measured with a Molecular Devices Versamax absorbance microplate reader every 20 minutes over the course of 18 h at 30°C with medium intensity shaking for 30 seconds prior to each reading. Each sample was analyzed in triplicates to obtain an average reading and standard deviation. The experiment was repeated three times. The normalized bacterial viability at each composite material as well as the antibiotic concentration was calculated using the following equation for a certain steady-state time point:[54]

($OD_{600}$ sample – $OD_{600}$ media control)/ ($OD_{600}$ negative control - $OD_{600}$ media control), where the media control is obtained from a HEPES buffer, and the negative control is obtained from bacterial exposure to water. The bacterial viability is proportional to the absorption of the sample at 600 nm ($OD_{600}$). A minimal or no decrease in bacterial viability is expected when the bacterial cells are exposed to a benign material. **Figure S8** shows the normalized bacterial viability of *Shewanella oneidensis* MR-1 when exposed to increasing concentrations ranging from 0 to 600 mg/L of the studied thermoelectric composite materials in water. It can be seen that all the composite materials do not adversely impact bacterial growth in this concentration range. The figure also shows the normalized bacterial viability of *Shewanella oniedensis* MR-1 when exposed to an antibiotic, kanamycin in water, which acts as a positive control, and it is seen that there is a significant decrease in viability at concentrations higher than 50 mg/L. Thus, it is concluded that should these thermoelectric devices degrade, leak, or are exposed to the natural aqueous environment post-use, they should be safe for the environment at exposure concentrations up to 600 mg/L.

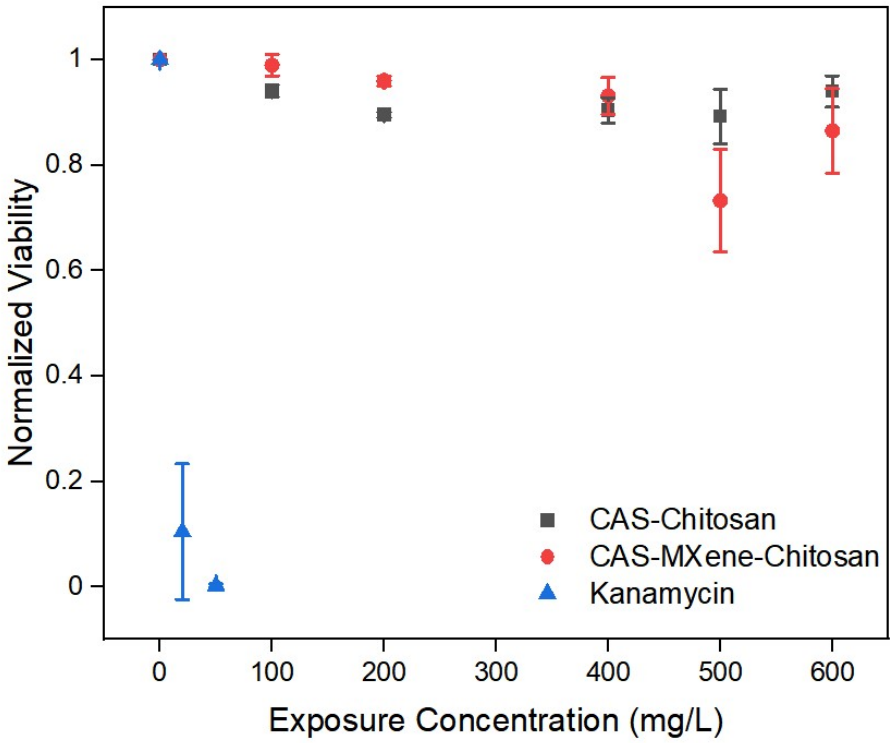


**Figure S9.** Normalized bacterial viability results of averaged biological triplicate samples of Chitosan-CAS and Chitosan-CAS-MXene inks (0-600 mg/L), and kanamycin antibiotic (0, 20, 50 mg/L) on *Shewanella oneidensis* MR-1.

## References


1. P. Banerjee, J. Huang, R.B. Ambade, E. Jang, M. Saeidi-javash, Y. Zhang, D. Madan, *Nano Energy,* 2021, **89**, 106482.

2. E. Jang, P. Banerjee, J. Huang, D. Madan, *Appl. Energy,* 2021. **294**, 117006.

3. J. Huang, R.B. Ambade, J. Lombardo, B. Brooks, A. Poosapati, P. Banerjee, M. Saeidi-Javash, Y. Zhang, D. Madan, *Appl. Mater. Today.*, 2024, **37**, 102116.

4. S.J. Kim, J.H. We, B.J. Cho, *Energy Environ. Sci.,* 2014, **7**, 1959.

5. F. Kim, B. Kwon, Y. Eom, J.E. Lee, S. Park, S. Jo, S.H. Park, B.S. Kim, H.J. Im, M.H. Lee, T.S. Min, K.T. Kim, H.G. Chae, W.P. King, J.S. Son, *Nat. Energy,* 2018, **3**, 301.

6. S.H. Park, S. Jo, B. Kwon, F. Kim, H.W. Ban, J.E. Lee, D.H. Gu, S.H. Lee, Y. Hwang, J.S. Kim, D.B. Hyun, S. Lee, K.J. Choi, W. Jo, J.S. Son, *Nat. Commun.,* 2016, **7**, 1.

7. S.J. Kim, H. Choi, Y. Kim, J.H. We, J.S. Shin, H.E. Lee, M.W. Oh, K.J. Lee, B.J. Cho, *Nano Energy*, 2017, 31, 258.

8. D. Madan, A. Chen, P.K. Wright, J.W. Evans, *J. Appl. Phys.,* 2011, **109**, 034904.

9. D. Madan, Z. Wang, A. Chen, R.C. Juang, J. Keist, P.K. Wright, J.W. Evans, *ACS appl. Mater. Interfaces*, 2012, **4**, 6117.

10. E. Jang, A. Poosapati, N. Jang, L. Hu, M. Duffy, M. Zupan, D. Madan, *Sci. Rep.,* 2019, **9**, 7869.

11. P. Banerjee, E. Jang, J. Huang, R. Holley, S. Vadnala, A. Sheikh, A. Trivedi, K. Jackson, V.K. Homman, D. Madan, *J. Electron. Mater.,* 2021, **50**, 2840.

12. E. Jang, A. Poosapati, D. Madan, *ACS Appl. Energy Mater.,* 2018, **1**, 1395.

13. E. Jang, P. Banerjee, J. Huang, R. Holley, J.T. Gaskins, M.S. bin Hoque, P.E. Hopkins, D. Madan, *Electronics,* 2020, **9**, 1.

14. T. Borca-Tasciuc, A.R. Kumar, G. Chen, Rev. *Sci. Instrum.,* 2001, **72**, 2139.

15. P. Liu, Y. Wen, C.F. Siah, M.E. Pam, B. Xu, A.V.Y. Thean, Y.K. Lim, S. Shin, *Appl. Phys. Lett.*, 2023, **122**, 252201.

16. S. Shin, R. Kumar, J.W. Roh, D.S. Ko, H.S. Kim, S. Il Kim, L. Yin, S.M. Schlossberg, S. Cui, J.M. You, S. Kwon, J. Zheng, J. Wang, R. Chen, *Sci Rep.*, 2017, **7**, 1.

17. G. Zheng, X. Su, H. Xie, Y. Shu, T. Liang, X. She, W. Liu, Y. Yan, Q. Zhang, C. Uher, M.G. Kanatzidis, X. Tang, *Energy Environ. Sci.,* 2017, **10**, 2638.

18. D.A. Polvani, J.F. Meng, N. V. Chandra Shekar, J. Sharp, J. V. Badding, *Chem. Mater.,* 2001, **13**, 2068.

19. Z. Wu, X. Chen, E. Mu, Y. Liu, Z. Che, C. Dun, F. Sun, X. Wang, Y. Zhang, Z. Hu, *Adv. Electron. Mater.,* 2020, **6**, 1900735.

20. C. Gayner, Y. Amouyal, *Adv. Funct. Mater.,* 2020, **30**, 1.

21. X. Lu, Q. Zhang, J. Liao, H. Chen, Y. Fan, J. Xing, S. Gu, J. Huang, J. Ma, J. Wang, L. Wang, W. Jiang, *Adv. Energy Mater.,* 2020, **10**, 1.

22. Z. Cao, M.J. Tudor, R.N. Torah, S.P. Beeby, *IEEE Trans. Electron Dev.,* 2016, **63**, 4024.

23. B. Paul, E.M. Björk, A. Kumar, J. Lu, P. Eklund, *ACS Appl. Energy Mater.,* 2018, 1, 2261.

24. D. Madan, Z. Wang, A. Chen, P.K. Wright, J.W. Evans, *Appl. Mater. & Interfaces,* 2013, **5**, 11872.

25. T. Varghese, C. Hollar, J. Richardson, N. Kempf, C. Han, P. Gamarachchi, D. Estrada, R.J. Mehta, Y. Zhang, *Sci Rep.*, 2016, **6**, 6.

26. T. Varghese, C. Dun, N. Kempf, M. Saeidi-Javash, C. Karthik, J. Richardson, C. Hollar, D. Estrada, Y. Zhang, *Adv. Funct. Mater.,* 2019, **30**, 1905796.

27. H. Choi, Y.J. Kim, C.S. Kim, H.M. Yang, M.W. Oh, B.J. Cho, *Nano Energy*, 2018, **46**, 39.

28. X. Lu, D.T. Morelli, Y. Xia, F. Zhou, V. Ozolins, H. Chi, X. Zhou, C. Uher, *Adv. Energy Mater.,* 2013,**3**, 342.

29. K. Suekuni, K. Tsuruta, M. Kunii, H. Nishiate, E. Nishibori, S. Maki, M. Ohta, A. Yamamoto, M. Koyano, *J. Appl. Phys.,* 2013, **113**, 043712.

30. T. Barbier, S. Rollin-Martinet, P. Lemoine, F. Gascoin, A. Kaltzoglou, P. Vaqueiro, A. V. Powell, E. Guilmeau, *J. Am. Ceram. Soc.,* 2016, **99**, 51.

31. Y. Yang, H. Hu, Z. Chen, Z. Wang, L. Jiang, G. Lu, X. Li, R. Chen, J. Jin, H. Kang, H. Chen, S. Lin, S. Xiao, H. Zhao, R. Xiong, J. Shi, Q. Zhou, S. Xu, Y. Chen, *Nano Lett.,* 2020, **20**, 4445.

32. Y. Xu, B. Wu, C. Hou, Y. Li, H. Wang, Q. Zhang, *Global Challenges,* 2024, **8**, 2300032.

33. Z. Lu, H. Zhang, C. Mao, C.M. Li, *Appl. Energy,* 2016, **164**, 57.

34. E. Mu, G. Yang, X. Fu, F. Wang, Z. Hu, *J. Power Sources,* 2018, **394**, 17.

35. Y.S. Jung, D.H. Jeong, S.B. Kang, F. Kim, M.H. Jeong, K.S. Lee, J.S. Son, J.M. Baik, J.S. Kim, K.J. Choi, *Nano Energy*, 2017, **40**, 663.

36. M. Saeidi-Javash, W. Kuang, C. Dun, Y. Zhang, *Adv. Funct. Mater.,* 2019, **29**, 1901930.

37. J.P. Rojas, D. Conchouso, A. Arevalo, D. Singh, I.G. Foulds, M.M. Hussain, *Nano Energy*, 2017, **31**, 296.

38. Z. Zhang, B. Wang, J. Qiu, S. Wang, *Manufacturing Lett.,* 2019, **21**, 28.

39. R. Roth, R. Rostek, K. Cobry, C. Köhler, M. Groh, P. Woias, *J. Microelectron. Syst*., 2014, **23**, 961.

40. M. Hyland, H. Hunter, J. Liu, E. Veety, D. Vashaee, *Appl. Energy*, 2016, **182**, 518.

41. T.N. Huu, T.N. Van, O. Takahito, *Appl. Energy,* 2018, **210**, 467.

42. Z. Cao, E. Koukharenko, R.N. Torah, J. Tudor, S.P. Beeby, *J. Phys.: Conference Series,* 2014, **557**. 1.

43. M. Takashiri, T. Shirakawa, K. Miyazaki, H. Tsukamoto, *Sensors and Actuators A: Physical,* 2007, **138**, 329.

44. H.B. Lee, J.H. We, H.J. Yang, K. Kim, K.C. Choi, B.J. Cho, Thin Solid Films. 2011, **519**, 5441.

45. L. Francioso, C.D. Pascali, I. Farella, C.Martucci, P. Cretì, P. Siciliano, A. Perrone, *J. Power Sources,* 2011, **196**, 3239.

46. A. Chen, D. Madan, P.K. Wright, J.W. Evans, *J. Micromech. and Microeng.,* 2011, **21**, 104006.

47. D. Madan, Z. Wang, A. Chen, R. Winslow, P.K. Wright, J.W. Evans, *Appl. Phys. Lett.*, 2014, **104**, 013902.

48. D. Madan, Z. Wang, P.K. Wright, J.W. Evans, *Appl. Energy*, 2015, **156**, 587.

49. Z. Cao, E. Koukharenko, M.J. Tudor, R.N. Torah, S.P. Beeby, *A: Physical,* 2016, **238**, 196.

50. D. Madan, Z. Wang, P.K. Wright, J.W. Evans, *Appl. Energy*, 2015, **156**, 587.

51. M.N. Hang, I.L. Gunsolus, H. Wayland, E.S. Melby, A.C. Mensch, K.R. Hurley, J.A. Pedersen, C.L. Haynes, R.J. Hamers, *Chem. Mater.*, 2016, **28**, 1092.

52. T.A. Qiu, T.H.T. Nguyen, N.V. Hudson-Smith, P.L. Clement, D.C. Forester, H. Frew, M.N. Hang, C.J. Murphy, R.J. Hamers, Z.V. Feng, C.L. Haynes, *Anal. Chem.,* 2017, **89**, 2057.

53. S. Sengupta, S.B. Ambade, T.L. O'Keefe, F. Tawakalna, J.K.H. Orbeck, R. J.Hamers, Z.V. Feng, C.L. Haynes, Z. Rosenzweig, *Environ. Sci.: Nano,* 2024, **11**, 627.

54. D.N. Williams, J.S. Saar, V. Bleicher, S. Rau, K. Lienkamp, Z. Rosenzweig, *ACS Appl. Bio. Mater.,* 2020, **3**, 1097.